Paleoceanography and Paleoclimatology

RESEARCH ARTICLE
10.1029/2023PA004717

A Warming Southern Gulf of Mexico: Reconstruction of Anthropogenic Environmental Changes From a *Siderastrea siderea* Coral on the Northern Coast of Cuba

M. Harbott[1], H. C. Wu[1], H. Kuhnert[2], C. Jimenez[3,4], P. González-Díaz[5], and T. Rixen[1,6]

[1]Leibniz Centre for Tropical Marine Research (ZMT) GmbH, Bremen, Germany, [2]MARUM—Center for Marine Environmental Sciences, University of Bremen, Bremen, Germany, [3]Enalia Physis Environmental Research Centre, Nicosia, Cyprus, [4]The Cyprus Institute, Nicosia, Cyprus, [5]Centro de Investigaciones Marinas Universidad de La Habana, Ciudad de La Habana, Cuba, [6]Institute of Geology, University of Hamburg, Hamburg, Germany

Key Points:

- A massive coral was used as a paleoclimatic and environmental archive for the reconstruction of sea surface temperature and $\delta^{18}O_{SW}$
- Reconstruction reaches back 160 years from 1845 to 2005 and shows a warming southeastern Gulf of Mexico (GOM) of 2.6–3.3°C
- A freshening of the southern GOM starting in the 1990s shows the onset of a phase shift to a positive Atlantic Multidecadal Oscillation

Supporting Information:

Supporting Information may be found in the online version of this article.

Correspondence to:

M. Harbott and H. C. Wu,
marie.harbott@leibniz-zmt.de;
henry.wu@leibniz-zmt.de

Citation:

Harbott, M., Wu, H. C., Kuhnert, H., Jimenez, C., González-Díaz, P., & Rixen, T. (2023). A warming southern Gulf of Mexico: Reconstruction of anthropogenic environmental changes from a *Siderastrea siderea* coral on the northern coast of Cuba. *Paleoceanography and Paleoclimatology*, *38*, e2023PA004717. https://doi.org/10.1029/2023PA004717

Received 27 JUN 2023
Accepted 29 SEP 2023

Author Contributions:

Conceptualization: M. Harbott, H. C. Wu
Data curation: C. Jimenez, P. González-Díaz, T. Rixen
Formal analysis: M. Harbott
Funding acquisition: H. C. Wu, T. Rixen
Methodology: M. Harbott, H. Kuhnert
Project Administration: H. C. Wu
Supervision: H. C. Wu
Visualization: M. Harbott
Writing – original draft: M. Harbott
Writing – review & editing: M. Harbott, H. C. Wu, H. Kuhnert, T. Rixen

Abstract

The Gulf of Mexico is a vital region for the Atlantic Meridional Overturning Circulation (AMOC), that fuels the exchange of heat between the tropics and the polar regions. A weakening of the AMOC would have dire consequences for the planet. First observations and ocean models show that this process has already started. Very limited knowledge of the components that are part of the AMOC such as the Loop Current (LC) make it difficult to understand its dynamics as well as changes in strength or temperature since the onset of the Industrial Revolution. Currently, there are no continuous in situ sea surface temperature or salinity measurements for the southeastern Gulf of Mexico or reconstruction attempts for this region, showing the necessity for high-resolution climate archives. A *Siderastrea siderea* coral core was retrieved from the northwestern Cuban coast and used as a sub-seasonally resolved sea surface temperature and hydroclimate archive. The approach is based on skeletal $\delta^{18}O$, and trace and minor element contents show an increase in temperature over 160 years since 1845 of 2.6–3.3°C. A possible stagnation of the warming trend set in after the 1980s, indicating a potential weakening of the Loop Current. Impacts in sea surface salinity such as El Niño events in the Pacific region can still be detected in the Gulf of Mexico as decreases in salinity in 1998 from the reconstructed $\delta^{18}O_{SW}$ coral record. In situ measurements remain crucial to understand the dynamics in the LC and its influence on the AMOC.

Plain Language Summary

The Atlantic Meridional Overturning Circulation (AMOC) is an important part of our climate system by exchanging heat between the Northern and Southern Hemispheres. Changes in its strength could have severe consequences for our climate system, like changes in rain patterns leading to droughts in Europe. The Gulf of Mexico (GOM) is supplying the AMOC with heat, it transports to the north. Due to the anthropogenic climate change, sea surface temperature and salinity of the GOM changed since the Industrial Revolution. However, measurements of these changes are rare. Paleoclimate and environmental archives such as coral cores can help to reconstruct those changes and better understand the anthropogenic climate change. Coral cores from massive corals act as archives and yield bi-monthly resolution, making it possible to reconstruct changes in seasonality as well as long-term trends. The coral core used in this study shows an increase in sea surface temperature of 2.6–3.3°C from 1845 to 2005. In the 1980s, we observe a halt in this increase in temperature pointing toward a weakening of the part of the AMOC in the GOM. It is important to understand the first signs of a weakening AMOC and its consequences for our climate system.

1. Introduction

The Atlantic Meridional Overturning Circulation (AMOC) is a crucial component of global ocean circulation (Boers, 2021; Dima et al., 2021). A projected decrease in the strength of AMOC will have profound impacts on global climate including a very likely AMOC strength decline in the 21st century. A rise in extreme event occurrences or abrupt climate change on human time scales are further alarming consequences of a weaker AMOC. The reason for the weakening AMOC can be found in the enhanced anthropogenic emission of CO_2 to the atmosphere and with that the warming of the ocean (Cheng et al., 2017; Roemmich et al., 2012). However, key information and understanding of the processes in the development of the AMOC since the 20th century remain unknown and impair our ability for more accurate predictions leading to larger uncertainties (Intergovernmental Panel On Climate Change, 2023). A continuous direct measurement of the AMOC started only in 2004, yet

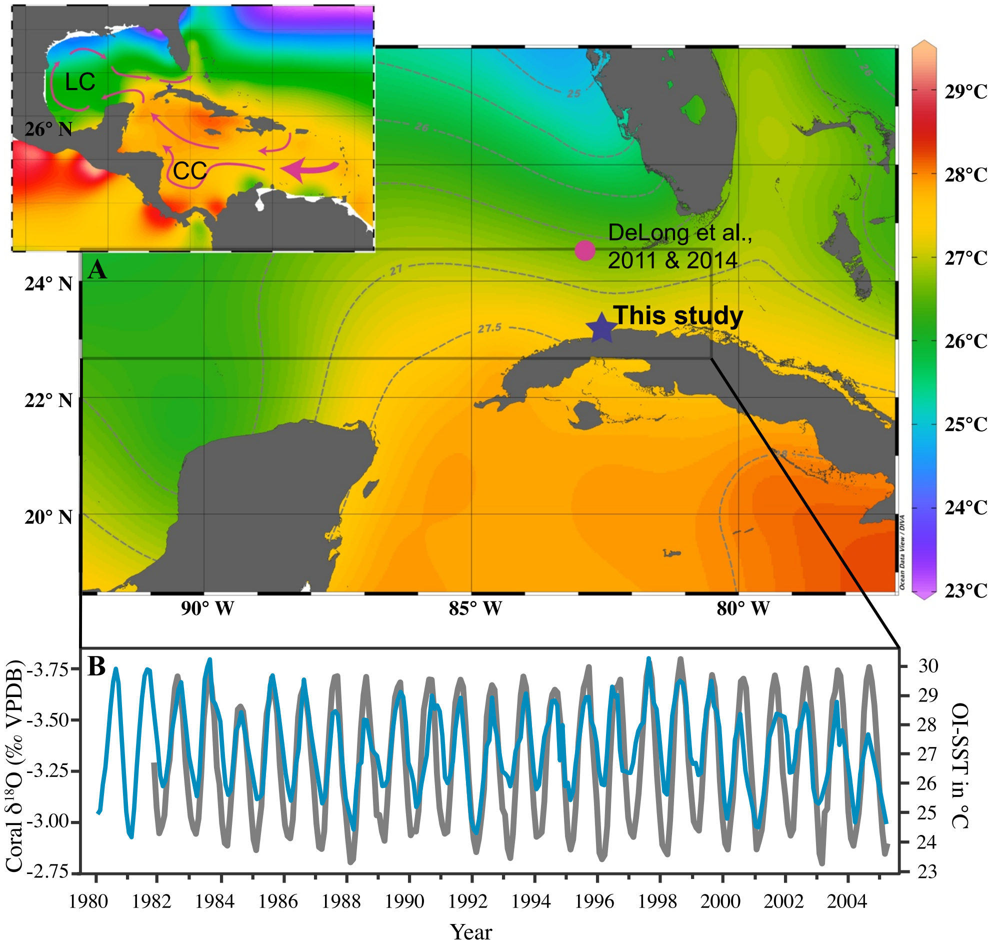

Figure 1. (a) Interpolated sea surface temperature (SST) (annual average from 1955 to 2017) temperature from the World Ocean Atlas 2018 1° × 1° grid in Ocean Data View. Red Arrows represent the Caribbean Current (CC) entering the Gulf of Mexico (GOM) via the Yucatan channel and transporting warm surface water to the GOM. The Loop Current (LC) exits the GOM and joins the Florida Stream (Gordon, 1967; Liu et al., 2012). (b) Light gray line representing OI-SSTv2.1 for the southern GOM from 80.5°W to 96.5°W and 22.5°N to 24.5°N compared to coral $\delta^{18}O$ (blue) from this study.

decadal and interdecadal fluctuations need a higher time span to be accurately represented (Caesar et al., 2021). Longer-term reconstructions of the AMOC have to be based on proxy data reconstructions (Caesar et al., 2021). Recent studies observed the first onsets of declining stability of the AMOC by changes in sea surface temperature (SST) and sea surface salinity (SSS) in the northern Atlantic Ocean (Boers, 2021; Caesar et al., 2021; Dima et al., 2021; Smeed et al., 2018).

One important component of the AMOC is the Caribbean Current that transforms into the Loop Current (LC) once it reaches the Gulf of Mexico (GOM; Figure 1). The LC enters the GOM via the Yucatan channel from the Caribbean Sea and joins the Florida Current, thereby providing the GOM with warm surface water (Figure 1). A decreased heat transport of the LC will result in reduced warming in the GOM (Liu et al., 2012). Thus, an overall weakening of the AMOC will lead to a weakened LC. However, the spatial and temporal distribution of SST and SSS for the GOM are not homogenous in their latitudinal distribution. Recent satellite-derived SST observations indicate a warming of the LC in the central GOM since 1985, whereas the shelf areas of Florida and Cuba indicate a cooling trend between 1985 and 2009 (Chollett et al., 2012).

1.1. Interannual and Interdecadal Oscillation

The tropical western Atlantic, the Caribbean basin, and the GOM are also influenced by competing forcings influencing SST and SSS records, notably the El Niño Southern Oscillation (ENSO), the North Atlantic Oscillation

(NAO), and the Atlantic Multidecadal Oscillation (AMO) (Enfield & Mayer, 1997; Giannini et al., 2001, 2000; Wang et al., 2008).

The ENSO teleconnection between the Pacific and Atlantic has different effects on different parts of the tropical Atlantic. During the mature phase of an ENSO event, a seesaw pattern between the sea level pressure (SLP) over the eastern Pacific and equatorial Atlantic forms. This SLP pattern leads to a divergent atmospheric flow over the Caribbean on a southwest-northeast axis from the convergent eastern Pacific during the mature phase of the ENSO (Giannini et al., 2000). While the ITCZ shifts further south in January and February of the following year of an ENSO event a negative SLP anomaly forms south of the eastern coast of the US, leading to intensified precipitation over the GOM (Giannini et al., 2000). The formation of the low SLP over the southern USA leads to weaker meridional atmospheric flow and an increase in SST over the Caribbean basin (Giannini et al., 2000). It has been shown that teleconnections across Central America induced precipitation changes in the Atlantic Ocean during EN years reacting to changes in the Pacific Ocean with a delay of one season (Giannini et al., 2000). While the ITCZ shifts further south in January and February of the following year of an ENSO event, a negative SLP anomaly forms off the south-eastern Coast of North America over the GOM, leading to intensified precipitation over the GOM. Cuba in the southern GOM will therefore be more likely to experience an increase in precipitation in the spring and summer after a severe EN event (Giannini et al., 2000). A clear signal of the ENSO teleconnection is not always visible in poxy data since counteracting forces such as the NAO might reduce the effect of ENSO on Caribbean precipitation.

During a positive NAO phase, the North Atlantic High is relatively strong during the winter leading to stronger trade winds in the equatorial Atlantic and with that to a cooling of the ocean's surface, counteracting the warming effect of a warm ENSO event (Giannini et al., 2001). A strengthening of a warm ENSO effect is observed when NAO is in a negative phase (Giannini et al., 2001).

The AMO is defined by oscillatory SST anomalies in the North Atlantic with coherent natural variability at 30–80 years. The positive (negative) phase of the AMO is associated with positive (negative) SST anomalies in the Atlantic Warm Pool (AWP), a large body of warm water including the GOM, the Caribbean Sea, and the western tropical North Atlantic (Wang et al., 2008). A warm phase of the AMO will lead to a larger AWP, which favors the formation of Atlantic tropical cyclones (Wang et al., 2008). Over the GOM the warm phase of the AMO is characterized by more precipitation compared to the cold phase (Goly & Teegavarapu, 2014). Cold AMO periods were registered approximately from 1900–1925, 1965–1994, while warm phases occurred from 1875–1899, 1926–1965, and 1995 to present (Alexander et al., 2014).

1.2. Current Best Practise

In situ continuous SST and SSS measurements are relatively sparse in the tropical oceans and especially in the southern GOM (Chollett et al., 2012). Moreover, the lack of long-term in situ measurements impedes the understanding of regional changes of the LC to project future trends of the region. Without such records, potential cooling or warming and weakening or strengthening of the LC in the GOM cannot be properly assessed and forecasted (DeLong et al., 2014; Liu et al., 2012). Additionally, extreme temperature changes due to the current anthropogenic climate change are already taking their toll on marine organisms, leading to mass coral bleaching events and thereby destroying entire coral reef ecosystems (Hughes et al., 2018). Besides providing the foundation of coral reef ecosystems, corals are also an important archive for reconstructing climate and environmental changes. By recording environmental factors such as SST and SSS in their skeletal materials, corals have been shown to be effective for the understanding of regional to large-scale ocean and climate variabilities.

Currently, several studies have published SST and SSS reconstruction from planktonic foraminifera in the GOM (Flower & Kennett, 1990; Lund & Curry, 2004; Poore et al., 2009; Richey et al., 2007, 2009; Schmidt et al., 2012). However, these sediment core-based records are only able to resolve climate at a low-resolution limiting our knowledge of seasonality, interannual, and interdecadal variability. The previously published high-resolution climate reconstructions from coral archives are also limited to the Dry Tortugas Island in the northern GOM (DeLong et al., 2011, 2014; Maupin et al., 2008). Furthermore, none of these studies attempted to reconstruct hydrological influences such as SSS, an important indicator for the strength of the AMOC (Boers, 2021; Dima et al., 2021). The studies conducted in the Dry Tortugas region point toward a stagnating warming after 1985, confirming a weakened warming in the GOM and with that a possible slowdown of the LC (DeLong et al., 2014).

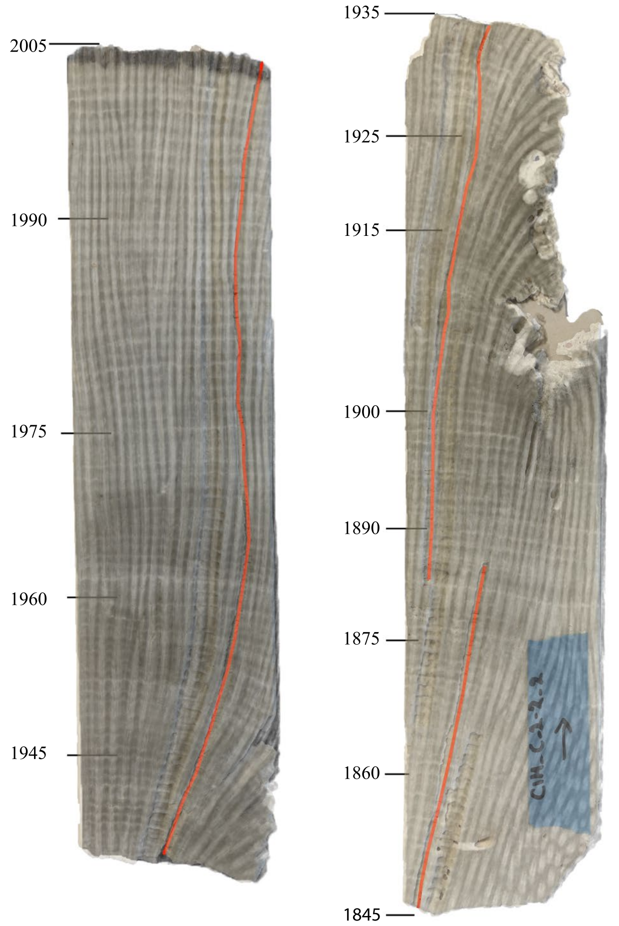

Figure 2. X-ray positive image laid over a photo of the sampled coral (wider sampling paths were sampled for yearly resolution and sampled over two polyps and are not included in this study) of the Cuban *Siderastrea siderea* coral core slabs with optimized sampling transects indicated in red following a single polyp thecal wall for most of the core across multiple slabs.

However, other studies and climate models indicate a warming of the southern GOM, including north of Cuba, only a few hundred kilometers away from Dry Tortugas (Chollett et al., 2012). To understand how large-scale and local climate phenomena influence these regions, local high-resolution climate reconstructions are necessary.

1.3. Scleractinian Corals as Climate Archives

Sr/Ca and δ^{18}O records of *Siderastrea siderea* have been verified as accurate and reliable climate archives in previous studies (DeLong et al., 2011, 2014; Guzmán & Tudhope, 1998; Maupin et al., 2008; Rodriguez et al., 2019). The coral-based proxy records have been shown to be in coherence with regional climate variability allowing for the development of long continuous records of reconstructed SST in the GOM region (DeLong et al., 2011, 2014; Maupin et al., 2008). Coral skeletal Sr/Ca and δ^{18}O ratios are the most widely used proxies for SST and hydroclimate (i.e., a mixture of freshwater and evaporation, and hence SSS). Coral skeletal δ^{18}O is dependent on SST and the δ^{18}O of seawater. By using Sr/Ca that is primarily temperature-driven, the temperature component in $\delta^{18}O_{coral}$ can be subtracted, yielding $\delta^{18}O_{SW}$ (Ren et al., 2003).

While growing, corals reflect the chemistry of the surrounding seawater in their aragonite skeletal composition. Cations in the ambient seawater, particularly those chemically similar to calcium (Ca^{2+}), such as strontium (Sr^{2+}), are incorporated in trace to minor amounts in the coral skeleton (Giannini et al., 2001). In relatively colder environments corals increasingly incorporate Sr and therefore the Sr/Ca ratio will rise (Smith et al., 1979). The Sr/Ca ratio of seawater is spatially homogenous with only minor depth gradients, and it is stable on the time-scale considered here (de Villiers et al., 1995).

1.4. Aim of the Study

This study uses a multi-proxy approach of a *S. siderea* coral to reconstruct changes in SST and δ^{18}Osw-SSS from the northern coast of Cuba. The coral archive and reconstructed climate variability span the period from 1845 to 2005. High-resolution reconstructions of climate variabilities have been scarce in this region. This study will calibrate and apply different coral-based proxy reconstructions of SST using the δ^{18}O values, and Sr/Ca relationship to assess the reliability of each proxy. Moreover, coral-based $\delta^{18}O_{sw}$ based on paired coral skeletal δ^{18}O and Sr/Ca is compared to gridded instrumental SSS. Finally, we aim to establish possible evidence of anthropogenic climate change imprint and the weakening signal of the AMOC in this region.

2. Materials and Methods

2.1. Coral Retrieval and Sampling

In July 2005, a 53 cm long coral core was collected from the center growth axis of a *S. siderea* colony off the northern coast of Havana, Cuba (82.4239°W, 23.1277°N; Figure 1) at 6 m depth. The sample was cored along the maximum growth axis of the coral to secure a continuous record and transported to the Leibniz Center for Tropical Marine Research (ZMT) in Bremen, Germany. Slabs measuring 5 mm were removed from the coral core half with X-radiograph imaging completed at the Zentrum für moderne Diagnostik (ZEMODI, Bremen, Germany) to reveal internal growth structure to guide sampling transect selection (Figure 2) (DeLong et al., 2013). The X-radiograph positive images revealed the density banding couplets of the coral as well as the orientation of the individual polyps. Prior to microsampling, the individual slabs were cleaned in an ultrasonic bath with 18.2 Ω milliQ water. Each individual wash lasted 5 min and the process was repeated for three wash cycles on each slab. The slabs were dried for at least 24 hr at room temperature. A continuous theca wall of an individual coral polyp identified on the X-ray images was microsampled by milling for skeletal powder material (Figure 2). The vertical linear extension rate of the *S. siderea* used in this study was 3–8 mm year^{-1}. The sampling intervals of 0.5 mm on the vertical growth axis yielded up to 1.5 mg of skeletal aragonite powder for bimonthly resolved geochemical analysis. The powder samples were collected with a Proxxon drill fitted with a 0.4 mm diameter diamond-tipped drill bit operated at low speed on an independent *x-y-z* directional stage. The sampling path is 1 mm in depth and 2 mm wide consisting of theca wall material. Although great care was taken to avoid admixtures from other skeletal elements, we cannot rule out that powder from the columella may have occasionally been included in minor amounts.

2.2. Stable Isotope Analysis

Stable isotope measurements were analyzed individually at 0.5 mm intervals at the MARUM-Center for Marine Environmental Sciences of the University of Bremen, Bremen, Germany. For each coral skeletal powder sample, approximately 60–120 µg of powder was dissolved in ∼105% H_3PO_4 at 75°C in an automated carbonate preparation device (Finnigan Kiel I or ThermoFisher Kiel IV), generating CO_2 gas that was then analyzed on a Finnigan MAT 251 or ThermoFisher MAT 253plus isotope-ratio mass spectrometer. Calibration and correction of offsets due to inter-machine differences were based on measurements of the Solnhofen limestone 2008 in-house standard, which itself was calibrated against NBS 19. The isotopic values are reported in ‰ versus the Vienna Peedee Belemnite reference scale. Repeat analyses of the house standard yielded a standard deviation of ±0.05‰ for $\delta^{18}O$. Following common practice, no correction was applied to account for the constant offset when measuring aragonite on a system calibrated with calcite.

2.3. Trace Elements Analysis

The elemental composition was measured on an Analytik Jena Plasma Quant MS Elite Inductively Coupled Plasma-Mass Spectrometer (ICP-MS) at ZMT from splits of the same coral skeletal powder as were the stable isotopes. Ultrapure 2% HNO_3 (2 mL) was added to digest 500 µg of coral skeletal powder, shaken and dissolved for at least 24 hr. An aliquot of 0.6 mL from the initial solution was diluted further with 0.6 mL of 2% ultrapure HNO_3 to reach a calcium concentration of approximately 50 ppm. An in-house internal coral standard (dissolved coral *S. siderea* skeleton from the north Cuban coast) as well as JCp-1 were diluted to reach a similar concentration in Ca of 50 ppm to be measured alongside the coral samples. To reduce interferences, we applied the internal gas mode for the isotopes ^{88}Strontium, ^{24}Magnesium, $^{43/44}$Calcium, ^{137}Barium, and ^{238}Uranium (Tech Note v1.17, Analytik Jena, 2017). The collision gas mixture of H_2 and He decreases the interferences and increases the signal-to-noise ratio. For the isotopes ^{7}Lithium and $^{10/11}$Boron, the application of the gas mode would lead to a loss of sensitivity, therefore the gas mode was not used for these two elements (Tech Note v1.17, Analytik Jena, 2017).

Certified single element stock solutions from Inorganic Ventures were used for the calibration of each individual element. Five calibration solutions of different concentrations for the different elements except Ca were prepared from one stock solution that was used over 1 week. Ca concentration remained the same for all calibration solutions and was added after diluting the stock solution to the different concentrations. After every fifth sample measurement on the ICP-MS, brackets of laboratory standards (a JCp-1, an in-house coral standard, and a consistency standard similar in concentration to our average value calibration solution) were measured to correct for instrumental drift (Schrag, 1999). Instrumental precision is ±0.35% relative standard deviation for Sr/Ca, 1.23% for Li/Mg, 0.36% for Mg/Ca, and 1.83% for U/Ca. For outliers, the measurement was repeated, and the average of all repetitions was calculated. Our average JCP-1 Sr/Ca value is 8.84 ± 0.03 mmol/mol (1σ, $n = 273$), 4.19 ± 0.015 mmol/mol for Mg/Ca (1σ, $n = 273$), 1.19 ± 0.02 µmol/mol for U/Ca (1σ, $n = 273$), and 1.6 ± 0.02 mmol/mol for Li/Mg (1σ, $n = 273$).

2.4. Chronology

We established an initial age model based on the clear annual density banding revealed by the X-radiograph positive image with the top of the colony corresponding to 2005, the year of collection (Figure 2). By comparing the estimated age to the seasonal variations in $\delta^{18}O$ and Sr/Ca, the depth to age relationship was confirmed. The highest $\delta^{18}O$ and Sr/Ca values correspond to the winter growing season and were assigned to February, the coldest month on average, and the lowest $\delta^{18}O$ and Sr/Ca values were assigned to August corresponding to the peak summer month. For the most recent record beginning in November 1981, the highest and lowest $\delta^{18}O$ and

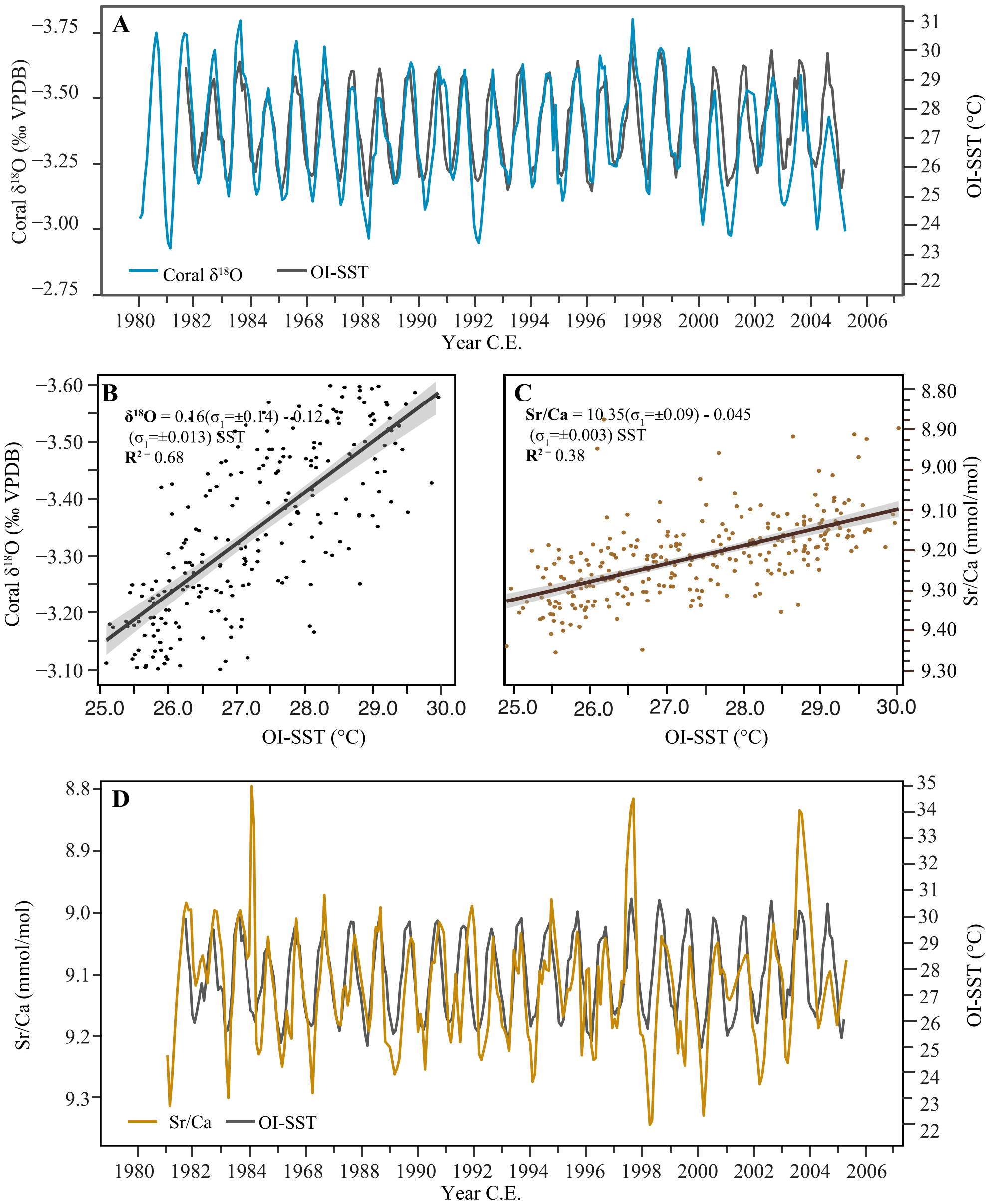

Figure 3. (a) Coral $\delta^{18}O$ ratios transformed to age domain, based on $\delta^{18}O$ age model, plotted with the gridded OI-SSTv2.1 product from the grid cell centered at 82.375°W and 23.125°N (Banzon et al., 2014; Huang et al., 2021). (b) Regression of Coral $\delta^{18}O$ and OI-SST (Banzon et al., 2014; Huang et al., 2021). (c) Regression of Coral Sr/Ca, based on Sr/Ca age model, and OI-SST (Banzon et al., 2014; Huang et al., 2021). The Pearson correlation coefficients as well as the regression equation are summed up in Table S1 in Supporting Information S1. The gridded product OI-SSTv2.1 was used for the calibration of the proxy due to the lack of instrumental records for this region. D-Sr/Ca ratios transformed to age domain, based on Sr/Ca age model, plotted with the gridded OI-SSTv2.1 product (Banzon et al., 2014; Huang et al., 2021).

Sr/Ca values were assigned to the coldest and warmest month respectively of the gridded OISSTv2.1 (Huang et al., 2021) (Figure 3a); the same was done for intermediate points in spring and autumn, provided the growth rate of the coral gave the necessary temporal resolution. For each year, two to four points were assigned to corresponding months from the OISSTv2.1 gridded data product (Huang et al., 2021).

The ages for the remaining samples were linearly interpolated based on spatial distances between age tie points, and X-radiograph imaging. Since both annual banding pattern, $\delta^{18}O$ and Sr/Ca seasonality are clear and regular, we do not consider the possibility of age errors on the time scale of years. However, the assumption that SST extremes always fall onto the same months introduces a noncumulative error of ±1 month for each sample.

For comparison with instrumental data and further statistical analyses, we interpolated our time series to equidistant, monthly, resolution using the Arand software Ager and Timer (Howell et al., 2006). Annual averages were calculated from these interpolated values. For anomaly calculations, the time interval from 1950 to 2000 was used as the reference period.

Outliers were identified through the outlier detection method provided by Chen and Liu (1993) on the by Arand interpolated geochemical data. The time series is described by a fitted general autoregressive moving average model. Outliers are identified in three steps: first, all potential outliers are identified based on preliminary model parameters, second, joint estimates of model parameters and outliers are detected and significant (threshold 0.001) outliers are removed and the parameter estimates are adjusted after removal of outliers. In the third step, the original series is filtered based on the adjusted parameters from step two and with the new residuals go through steps 1 to 2. The linear regression methods were then used on the outlier corrected data.

The geochemical and isotopic time series of this *S. siderea* coral span from 1845 to 2005 for a total of 160 years.

2.5. Calibration to SST

Coral $\delta^{18}O$ and Sr to Ca ratios were calibrated to the 0.25° by 0.25° gridded OI-SST (Banzon et al., 2014; Huang et al., 2021, High-Resolution SST data provided by the NOAA/OAR/ESRL PSL, Boulder, Colorado, USA, from their Web site at https://www.ncei.noaa.gov/data/sea-surface-temperature-optimum-interpolation/v2.1/access/avhrr/) centered at 82.375°W and 23.125°N. The calibration period is 1981–2005 (Figure 3). We chose to only display $\delta^{18}O$ and Sr/Ca results for their robust regressions to OI-SSTv2.1 (Banzon et al., 2014; Huang et al., 2021). Additional element to Ca ratios calibrated to OI-SST based on the $\delta^{18}O$ and Sr/Ca age models can be seen in the supplementary materials Tables S1a and S1b in Supporting Information S1.

Outlier detection was based on the iterative outlier detection and adjustment procedure of Chen and Liu (1993) and incorporated into the R package "*Forecast*" (Hyndman & Athanasopoulos, 2018). It was applied to the time series generated by Arand (further explanation of how Arand was used, can be found in Section 2.5) (Howell et al., 2006). The ordinary least squares (OLSs) regression method has been one of the most commonly used regression techniques for the development of the reconstruction of SST from element to Ca ratios and $\delta^{18}O$. This regression technique only assumes an error for the dependent variable and an error of zero for the independent variable, while other regression methods such as weighted least squares, reduced major axis, and bootstrapped weighted least squares developed by Xu et al. (2015) account for errors on both axes. Unfortunately, there is still no common approach for the coral-based paleoceanography community on which technique to use thus leading to differences in regressions for the same species and regions (Xu et al., 2015). After testing the data for homoscedasticity, the OLS method was chosen.

Error assessment for the Sr/Ca and $\delta^{18}O$ to SST calibration can be reviewed in supplementary materials. The analytical errors of Sr/Ca and $\delta^{18}O$ were propagated with the in Table S1 in Supporting Information S1 reported regression errors and yielded the overall errors of ±0.05°C for $\delta^{18}O$ and 0.26°C for Sa/Ca.

2.6. Reconstructed $\delta^{18}O_{SW}$

$\delta^{18}O$ of seawater ($\delta^{18}O_{SW}$) reconstruction from coral skeletal $\delta^{18}O$ ($\delta^{18}O_C$) assumes that $\delta^{18}O_{Coral}$ is a function of both SST and $\delta^{18}O_{SW}$, while variations in Sr/Ca depend on SST primarily. Thus, the reconstruction method as described by Ren et al. (2003) is important to note that instantaneous changes in $\delta^{18}O_C$ are the sum of two components, where one component describes the changes in SST, whereas the other contribution influences instantaneous changes in $\delta^{18}O_{SW}$ (Ren et al., 2003).

$$\begin{aligned} \triangle\delta^{18}O_C &= \triangle\delta^{18}O_{(SST\,contribution)} + \triangle\delta^{18}O_{(SW\,contribution)} \\ &= \triangle\left(\partial\delta^{18}O_{(C)}/\partial SST\right)^{*}\triangle SST \\ &\quad + \left(\triangle\partial\delta^{18}O_{(C)}/\triangle\partial\delta^{18}O_{(SW)}\right)^{*}\triangle\delta^{18}O_{SW}, \end{aligned} \tag{1}$$

$\triangle\partial\,\delta^{18}O_{(C)}/\partial SST$ is the rate of change of −0.22‰ per °C for the formation temperature of carbonates and the oxygen isotopic equilibrium, a mean based on 19 coral calibrations (Lough, 2004). For Siderastrea coral, a slope of −0.043 mmol/mol per °C was applied, following the master coral regression of DeLong et al. (2014) for the rate of change $\triangle\partial\,\delta^{18}O_{(C)}/\triangle\partial\,\delta^{18}O_{(SW)}$. Equation 1 only yields relative changes instead of absolute values. By adding up the changes gained by Equation 1 to the $\delta^{18}O_{SW}$ reference value from the GOM of 1.84‰, it is possible to reconstruct the variation for this region (Lowenstam & Epstein, 1957). Error propagation can be found in the

Supporting Information. The error for $\delta^{18}O_{SW}$ ±0.2 ‰ and was calculated from the combined error of the analytical errors of $\delta^{18}O$ and Sr/Ca as well as the calibration errors from the OLS regressions.

2.7. Pseudo Coral Forward Modeling

Variations in $\delta^{18}O_C$ depend on both local SST and $\delta^{18}O_{SW}$ at the time of growth. In order to estimate the influence of both environmental factors on coral skeletal $\delta^{18}O$ ratios, a forward modeling exercise was applied by generating a pseudo-coral model. A pseudo-coral proxy or pseudo-coral forward model is a bivariate model comparing observed $\delta^{18}O_C$ with predicted $\delta^{18}O_C$ from a linear model driven by instrumental data of the 20th century (Thompson et al., 2011). This bivariate model yields the following equation (Thompson et al., 2011):

$$\delta^{18}O_{\mathrm{Pseudocoral}} = a_1\,\mathrm{SST} + a_2\,\mathrm{SSS} \tag{2}$$

where $a_1 = -0.22$ ‰ °C^{-1}, describing the effect of formation temperature on carbonate oxygen isotopic composition (Lough, 2004), and a_2 is the empirical slope of $\delta^{18}O_{SW}$ versus SSS (0.15 ‰ per salinity unit) for the tropical Atlantic reported by LeGrande and Schmidt (2006). The SST and SSS used for this model are from the following instrumental data products: SST, OI-SSTv2.1 (Banzon et al., 2014; Huang et al., 2021); SSS, SODA v2.1.6 (Carton & Giese, 2008).

3. Results and Discussion

3.1. Age Model Comparison of $\delta^{18}O$ and Sr/Ca With Instrumental SST

In this study, we developed two different age models based on $\delta^{18}O$ and the more established Sr/Ca (Figure 3) (DeLong et al., 2011, 2014; Fowell et al., 2016; Maupin et al., 2008; Weerabaddana et al., 2021). In addition, the Sr/Ca-OI-SST slope (for the Sr/Ca age model) fits into the slope range reported by DeLong et al. (2011) with a rate of change of 0.045 mmol/mol per °C (±0.003°C) (Figure 3c). Both reconstruction attempts (based on the $\delta^{18}O$; Figures 3a and 3b; and Sr/Ca-age models; Figures 3c and 3d) show an increase in temperature from 1845 to 2005. Although Sr/Ca is the more established proxy for temperature reconstruction for this region, $\delta^{18}O$ shows a more promising fit for the OI-SST regression (Tables S1 and S3 in Supporting Information S1) (Delong et al., 2011, 2014; Fowell et al., 2016; Maupin et al., 2008; Weerabaddana et al., 2021) (all results for both age models can be found in Tables S1–S7 in Supporting Information S1). The better fit to OI-SSTv2.1 might be due to the highest temperature occurring during the same month as the maximum precipitation rate (Jury et al., 2007), since $\delta^{18}O$ is both, a proxy for temperature and $\delta^{18}O_{SW}$ (Ren et al., 2003). The pseudo coral model shows a correlation coefficient between the model and OI-SSTv2.1 of 0.98, indicating a stronger influence of SST on the corals $\delta^{18}O$. Therefore, we have decided to base our analysis on the $\delta^{18}O$ age model. All results based on the Sr/Ca age model can be found in the supplementary materials.

The two age models developed for this study based on $\delta^{18}O$ and Sr/Ca agree on an increase in temperature over the 160 year time span from 1845 to 2005. For the respective grid cells encompassing our location, both OI-SST (1988–2005) and ER-SST (1854–2005) indicate no significant increase in SST (Banzon et al., 2014; Huang et al., 2021, 2017). This disagreement between coral-based SST and gridded SST products has been previously observed in the Caribbean and across many other regions in the Pacific (Evans et al., 2000; Kilbourne et al., 2008; Vásquez-Bedoya et al., 2012). The discrepancy between coral SST reconstructions and the gridded SST data of OI-SST and Extended Reconstructed SST version 4 (ER-SST; Huang et al., 2017) may be due to the spatial averaging of the SST values across the grid cell. By using gridded SST products instead of in situ measurements, local SST signals are suppressed by averaging over 2° by 2° (ERSST) or 0.25° by 0.25° (OI-SST). Furthermore, we would not recommend using annually averaged data for the calibration of temperature proxies since this would lead to a loss of information for the extreme values. Unfortunately, in situ measurements are not available for the northern Cuban coast. Despite the lack of similar secular trends, verification of our coral-based $\delta^{18}O$-SST reconstruction with the gridded ER-SST yields a correlation coefficient of (r) = 0.54 for the period 1854–2005. Another significant correlation ($r = 0.36$; $p < 0.001$) was also recorded between Sr/Ca-SST and ERSST.

3.2. Warming of the Southern GOM

Illustrating the quality of the massive coral's ability to record SST, the environmental proxies derived from this northern Cuba *S. siderea* coral skeletal $\delta^{18}O$, Sr/Ca, U/Ca, Mg/Ca, and Sr-U all indicate strong correlations to SST (Table S2 in Supporting Information S1). SSTs reconstructed over the period 1845–2005 differ between proxies, with the overall warming ranging from 0.7°C to 3.32°C (±0.21°C), equivalent to 0.04–0.21°C per decade (Figures 4 and 5 and Figure S1 in Supporting Information S1).

10.1029/2023PA004717

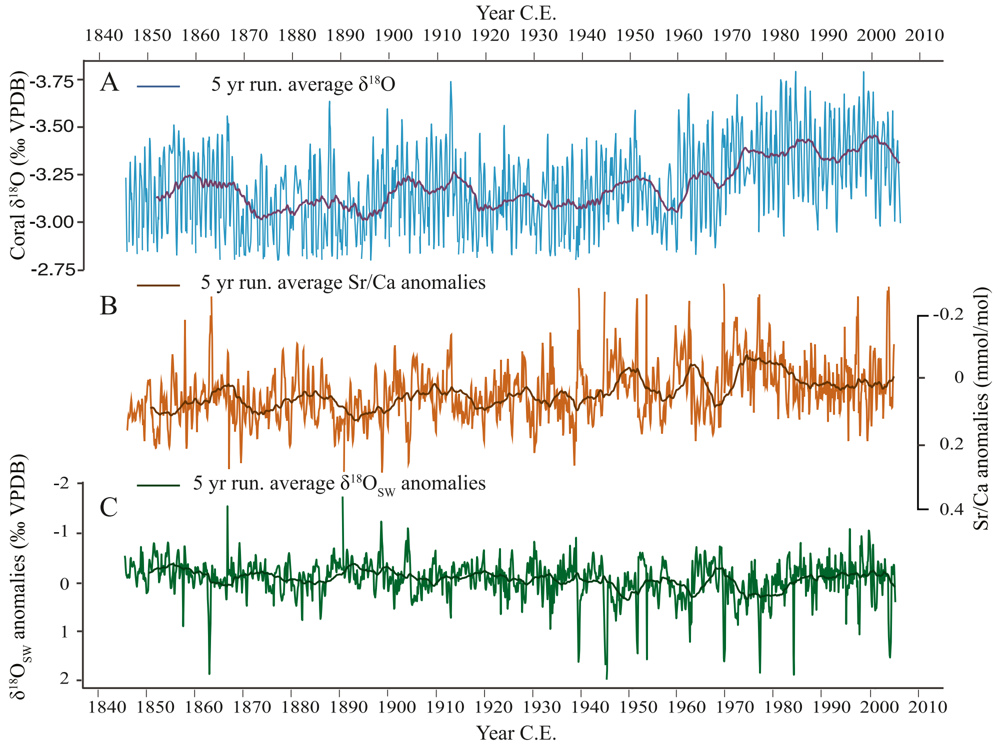

Figure 4. (a) $\delta^{18}O$ inversely plotted and transformed into the age domain with a 5 years running average plotted at the end of the respective 5 years period. Total temperature increase from linear regression in Table 1 is 2.6°C over 160 years. (b) Sr/Ca anomalies with 5 years running averages plotted at the end of the respective 5 years period. Anomalies were calculated with the climatological mean from 1950 to 2000. A temperature increase of 3.3°C from the regression in Table 1 over 160 years was calculated. (c) $\delta^{18}O_{SW}$ ratios were calculated with $\delta^{18}O$ and Sr/Ca (Equation 2). Anomalies were calculated with the climatological mean from 1950 to 2000.

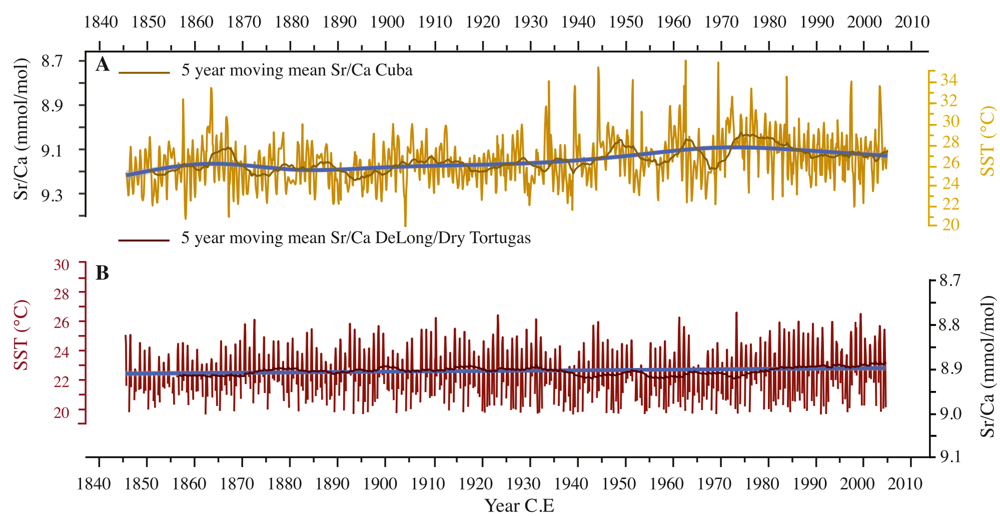

Figure 5. (a) Sr/Ca (based on the $\delta^{18}O$ age mode) and reconstructed temperatures from Sr/Ca regression. (b) Master Coral record from DeLong et al. (2014), averaged of Sr/Ca time series of three different corals from the Dry Tortugas National Park.

Table 1
Trend of Temperature and Hydroclimate Proxies Over Time and Their Significance and Change Per Decade in °C for Each Proxy Reconstructed SST

Proxy	*r*	*p*-value	Trend over time	Total temperature increase from linear regression °C
$\delta^{18}O_{coral}$	−0.4	**<0.001**	$\delta^{18}O = -0.002\ (\pm 0.0001)\ yr + 0.52\ (\pm 0.19)$	0.16
$\delta^{18}O_{SW}$	0.18	**<0.001**	$\delta^{18}O_{SW} = -0.0014\ (\pm 0.0002)\ yr - 1.12\ (\pm 0.40)$	
$\delta^{18}O_{pseudo}$	−0.05	0.09	$\delta^{18}O_{pseudo} = -0.003\ (\pm 0.004)\ yr + 8.05\ (\pm 7.23)$	0.20
Sr/Ca	−0.28	**<0.001**	Sr/Ca = −0.0007 (±0.00004) yr + 10.51 (±0.94)	0.21
Li/Mg	0.03	0.19	Li/Mg = 0.00009 (±0.00007) yr + 1.63 (±0.01)	−0.03
U/Ca	−0.24	**<0.001**	U/Ca = −0.0004 (±0.00003) yr + 2.00 (±0.06)	0.15
Mg/Ca	0.33	**<0.001**	Mg/Ca = 0.002 (±0.0001) yr + 0.06 (±0.23)	0.30
Sr-U	−0.24	**<0.001**	Sr-U = −0.0004 (±0.00004) yr + 9.95 (±0.07)	0.04

Note. The year variable refers to the year and decimal month. *r* is the Pearson correlation coefficient. Bold *p*-values indicate a significant *p*-value for Trend over time.

The magnitude of SST change reconstructed from Sr/Ca and $\delta^{18}O$ from the southern GOM (Figures 4a and 4b) in this study appears relatively larger compared to previous studies conducted in the northern GOM at Dry Tortugas (DeLong et al., 2014; Maupin et al., 2008). Taking the more conservative regression equations of previous studies from the northern GOM and the data of this study yields a temperature increase of 0.95°C–2.38°C from 1845 to 2005 (DeLong et al., 2014; Maupin et al., 2008). In the western Caribbean Sea on the Mesoamerican Barrier Reef of Belize, the temperature increase based on Sr/Ca-SST was similarly consistent with only a warming of 0.05–0.14°C per decade over the past 160 years (Fowell et al., 2016). The most extreme temperature increase in the southern GOM is found from the $\delta^{18}O$- and Sr/Ca-SST of this study with a rate of warming equaling 2.62 (±0.05°C)to 3.32 (±0.21)°C (3.32°C for Sr/Ca) or 0.21°C per decade. Although coral $\delta^{18}O$ is reflecting the combined changes in SST and $\delta^{18}O_{SW}$, the magnitudes of the SST increase reconstructed from $\delta^{18}O$ and Sr/Ca agree.

To further verify coral $\delta^{18}O$ sensitivity to SST at this location, a forward modeling approach using a pseudo-coral model (Dee et al., 2017; Thompson et al., 2011) was tested and confirmed that local SST can explain up to 98% of the variability in coral skeletal $\delta^{18}O$. This validates the fidelity of *S. siderea* coral skeletal $\delta^{18}O$ as a stronger recorder for SST at this location than for $\delta^{18}O_{SW}$ and parallel salinity changes. However, a difference in the temperature trend can be observed between $\delta^{18}O_{coral}$ and $\delta^{18}O_{pseudocoral}$. The pseudo coral forward model exhibits no significant ($p = 0.09$) temperature trend over the 160 years of reconstructed record.

At Dry Tortugas in the northern GOM, DeLong et al. (2014) reported a significant temperature increase of 0.7°C from 1952 until 1985 based on a reconstruction from a *S. siderea* coral core. This late 20th century trend is in agreement with our data from the southern GOM of Cuba with a contemporaneous warming between 0.49°C based on Sr-U-SST up to 0.68°C from Sr/Ca-SST (Table 2).

A visual shift (Figures 4 and 5) in reconstructed SST can be observed after 1980, where the reconstructed $\delta^{18}O$-SST reached a plateau equating to a pause in warming. Reconstructed Sr/Ca-SST and Sr-U SST even suggest a slight decrease in SST up to the year 2005. Quantifying the significance of this change is difficult due to the shortness of this trend at the end of the record. However, the results are consistent with the findings of DeLong et al. (2014) who described a discontinuation of warming SST after 1985 and attributed it to the possible slowdown of the LC.

3.3. Long-Term SST Trend Linked to LC and AMOC

Ocean models show a weakening of the LC that is consistent with the 20%–25% reduction of the AMOC strength from the late 20th century to the late 21st century (Liu et al., 2012). Multiple proxy records produced by Caesar et al. (2021) based on changes in the heat transport reconstructed from a variety of ocean and land-based proxies (sortable silt data, coral, foraminifera, tree rings, ice cores), suggest an unprecedented decline in the last 2,000 years of AMOC strength since the 20th century. Evidence indicating a weakening of the AMOC such as the Florida Current and the GOM transport has declined the fastest during the last two decades (Piecuch, 2020).

Table 2
Correlations of Multiple Proxies to OISSTv2 (Banzon et al., 2014; Huang et al., 2021) and Their Corresponding Significance (p) and Pearson Correlation Coefficient

Proxy	r	p-value	SST-proxy	Change per decade in °C
$\delta^{18}O$	0.83	<0.001	$\delta^{18}O = -0.16\ (\pm 0.14) - 0.12\ (\pm 0.013)$ SST	0.16
Sr/Ca	0.47	<0.001	Sr/Ca = $10.04\ (\pm 0.8) - 0.03\ (\pm 0.003)$ SST	0.21
Li/Mg	0.35	<0.001	Li/Mg = $2.67\ (\pm 0.32) - 0.03\ (\pm 0.004)$ SST	−0.03
$\delta^{18}O_{pseudo}$	0.99	<0.001	$\delta^{18}O_{pseudo} = 5.44\ (\pm 0.21) - 0.22\ (\pm 0.009)$ SST	0.20
U/Ca	0.50	<0.001	U/Ca = $1.94\ (\pm 0.12) - 0.02\ (\pm 0.001)$ SST	0.15
Mg/Ca	0.30	<0.001	Mg/Ca = $2.17\ (\pm 0.56) + 0.06\ (\pm 0.02)$ SST	0.30
Sr-U	0.47	<0.001	Sr-U = $9.88\ (\pm 0.59) - 0.03\ (\pm 0.002)$ SST	0.15

Note. Change per decade is based on the OISSTv2 regressions.

While the LC still warms the southern GOM, it does not reach the northern GOM due to the weakening. The longer-term trend for the northern GOM is confirmed by 25 years of satellite data. The warm Caribbean basin water still reaches the southern GOM leading to a warming in that region (Chollett et al., 2012). It is possible that a lack of in situ measurements in the southern GOM as well as the averaging of SSTs in gridded data biased toward a loss of warming trend of the southern GOM.

Summer warming has increased more than winter warming leading to a larger seasonality as observed by satellite data for the Caribbean Sea and the GOM (Chollett et al., 2012). This is in agreement with the reconstructed SST observed from our coral colony. While the seasonal amplitude before a calculated change point in 1968 was 2.49°C, it increased to 3.26°C after 1968 (based on the seasonality means of all proxies and a change point analysis based on a detection algorithm provided in the R package Strucchange) (Otto, 2019; Zeileis et al., 2002). The observed hiatus of the warming trend may be indicating a slowdown of the LC, in agreement with the observations of DeLong et al. (2014) from the northern GOM due to a possible weakening of the AMOC (Boers, 2021; Dima et al., 2021). However, the extended OI-SST record for this northern Cuba location indicates the resumption of a significant increase in SST ($p < 0.05$) after 2005 for the period 1981–2019 (Reynolds et al., 2002). A similar significant warming trend ($p < 0.05$) can be observed in another gridded SST product between 1981 and 2021 (ERSST v5; Huang et al., 2017). While other regions, such as the Caribbean Sea, exhibit increasing temperatures of up to 0.5°C per decade (Chollett et al., 2012), the southeastern as well as the northern GOM indicate no warming from the 1980s onward. Other studies have linked such a stop in warming with a decline in the strength of the LC and with that of the AMOC (DeLong et al., 2014; Liu et al., 2012). However, such a decline, as hypothesized by DeLong et al. (2014) needs to be verified with instrumental records and cannot solely be based on reconstruction efforts. Our coral-based reconstructed SST records may possibly be indicating the slowdown of the LC and with it a decline in the warming of the GOM. The noteworthy global warming trend continues unimpeded in other regions of the Caribbean and the western Atlantic (Caesar et al., 2018).

3.4. Interannual, Interdecadal, and Multidecadal Variability

Other coral-based proxy records from the Caribbean region have revealed significant interannual variability following signal processing with singular spectrum analysis (SSA) (Giry et al., 2012; Kilbourne et al., 2008). However, the proxy records from this study did not reveal significant frequencies from SSA. Although no significant spectral peaks could be identified, component analysis revealed interannual variabilities in all proxy records. All SST indicators in this study show a 3–7 years interannual variability pointing toward the ENSO teleconnection between the Pacific and Atlantic Ocean (Giry et al., 2012). Eleven percent of the variability can be attributed to the 3–7 years band for $\delta^{18}O$ and 22% for Sr/Ca.

SSA (Vautard & Ghil, 1989) does not identify significant interdecadal to multidecadal components in the proxy time series (Figures S2–S6 in Supporting Information S1). However, component analysis shows that 11% of the variability in $\delta^{18}O$ can be explained by a 33-year cycle, while Sr/Ca shows a 16-year variability (17%). Multidecadal variabilities between 30- and 70-year in the Atlantic are often connected to the AMO. Recent studies however, have suggested that multidecadal oscillations could be an artifact of volcanic eruptions (Mann

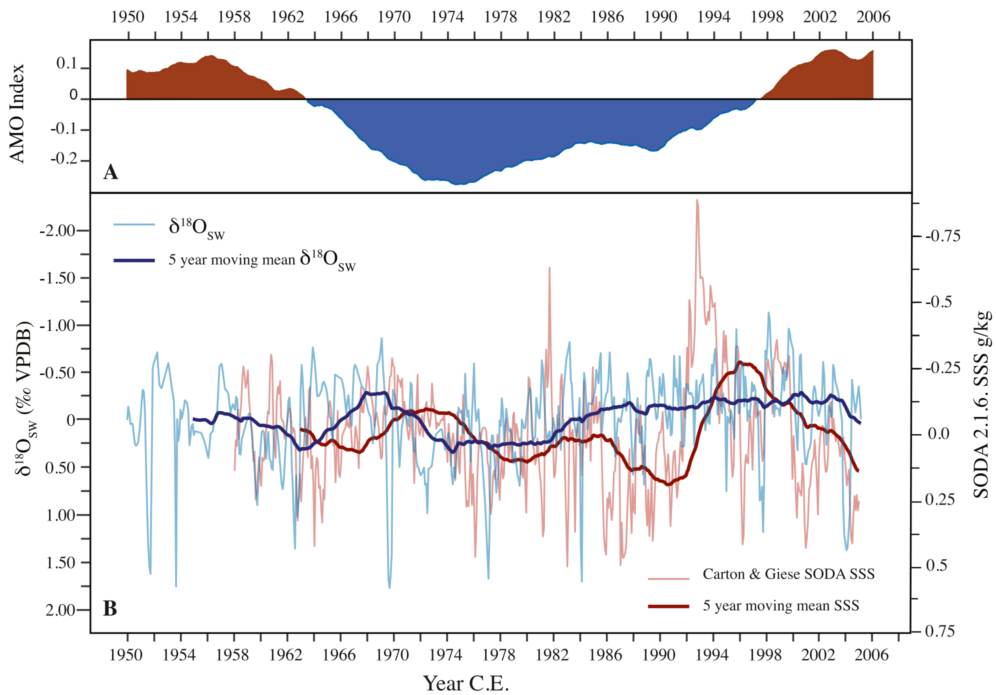

Figure 6. (a) Atlantic Multidecadal Oscillation (AMO) index (Enfield et al., 2001). The positive AMO index is colored red and represents the warm AMO phases. The blue negative AMO part is the cold AMO period. (b) Reconstructed detrended $\delta^{18}O_{SW}$ in light blue. The dark blue line represents the 5 years smoothed $\delta^{18}O_{SW}$ (±0.2‰) ratios. Seasonal detrended sea surface salinity (SSS) values from Carton and Giese (2008) are shown by the light red line, while the dark red line is the 5 years smoothed SSS signal.

et al., 2021). Furthermore, anthropogenic warming might overprint warming effects of warm or cool phases during the last century of the AMO, thereby producing the differences in observed and reconstructed AMO oscillation patterns (Mann et al., 2021). The length of our coral record (160 years) limits detection of variance in the AMO band to the short-period end (~30 years).

3.5. Hydroclimatology

By removing the temperature effect from $\delta^{18}O_{coral}$ using paired $\delta^{18}O_{coral}$ and Sr/Ca-data, we have reconstructed $\delta^{18}O_{SW}$ (Figure 4c). In previously published paired coral $\delta^{18}O$ and Sr/Ca records, $\delta^{18}O_{SW}$ has been shown to be a reliable proxy for SSS in regions dominated by changes in SST and $\delta^{18}O_{SW}$ due to changes in SSS (Gagan et al., 2000, 1998; Ren et al., 2003). Over the 47-year period between 1958 and 2005, reconstructed $\delta^{18}O_{SW}$ indicate a reduction by 0.016 ‰ that translates into a freshening of the surface water of −0.081 g/kg. Qualitatively, this agrees with the SODA SSS (Carton & Giese, 2008), but underestimates the change of −0.311 g/kg indicated by the latter (Figure 6). This discrepancy might again be due to the size of the SSS grid taking a bigger region into account than what is represented by our coral.

However, correlation between reconstructed monthly $\delta^{18}O_{SW}$ and SODA SSS v.2.1.6 (Carton & Giese, 2008) is not as robust as the coherence between coral $\delta^{18}O$-SST and ER-SST, with SSS explaining less than 1% of the variability in the results. To reduce the influence of high-frequency noise, we also compared the 5-year moving means of SODA SSS and $\delta^{18}O_{SW}$. Filtering out the noise by comparing the smoothed $\delta^{18}O_{SW}$ data to the SSS-SODA data set shows better correlation (e.g., 10 years smoothing correlated well to the SSS data set with a Pearson correlation coefficient of 0.66, $p < 0.001$, Table S7 in Supporting Information S1). While monthly variability is not well captured by the coral, long term trends are reflected in the $\delta^{18}O_{SW}$ data. Over ENSO timescales, the gridded SSS data set shows a minimum of 35.13 g/kg in late autumn of 1992 while the reconstructed $\delta^{18}O_{SW}$ shows a minimum of 0.85 ‰ (equivalent to 32.32 g/kg) for the summer of 1999. In January 1992 and December 1998, two of the more severe EN events categorized by the extended Multivariate ENSO index were documented in the Pacific Ocean (Wolter & Timlin, 2011). The low SODA SSS as well as the low $\delta^{18}O_{SW}$ values

10.1029/2023PA004717

in late 1992 and 1999 were likely induced respectively by the central and eastern Pacific EN event and atmospheric teleconnection to the Atlantic altering the precipitation pattern in the following months (Figure 6). Due to the 0.5° by 0.5° grid size of the SODA SSS gridded product, a wider region is taken into account for the SSS values, leading to lower salinity values in 1992 when the coral did not record its lowest values. The Caribbean Sea experiences high precipitation later in the year than the GOM, thereby potentially influencing the SSS data set (Giannini et al., 2000).

The running mean in Figure 6b as well as binned $\delta^{18}O_{SW}$ data over the entire time span in Figure S7 in Supporting Information S1 indicate significant differences in means ($p < 0.001$) for the late 20th century. A change point analysis revealed a significant ($p < 0.05$) change in mean in 1980 to lower values (Otto, 2019; Zeileis et al., 2002). A shift to lower salinity values corresponds to lower $\delta^{18}O_{SW}$ ratios reaching its peak in the early 1990s, which also coincides with a change in phase of the AMO index (Figure 6) (Enfield et al., 2001) and an increased tendency to more biennial Central Pacific ENSO events (Cai et al., 2019). The time period in the early 1990s also witnessed a shift to more central Pacific EN events with SST warming located in the central equatorial Pacific compared to the conventional canonical EN with SST warming in the eastern Pacific (Goly & Teegavarapu, 2014; Yu et al., 2015). Thus, the combination of a strong EN event in 1992 and 1998 as well as the shift in AMO could possibly explain the increase in precipitation and associated change in salinity in the southern GOM during this time (Figure 6). The decrease observed in $\delta^{18}O_{SW}$, especially in the 1990s as well as in the gridded SSS data might therefore partly be explained by a shift in the phase of the AMO. The change point analysis for $\delta^{18}O_{SW}$ shows a shift in $\delta^{18}O_{SW}$ mean before the AMO index changes. Under the aspect that the correlation between AMO indices and paleoclimate records show no correlation for the preindustrial period and correlation since (Kilbourne et al., 2008), longer records for the southern GOM are needed to verify this link between the AMO and coral SST records.

Due to the oscillatory character of AMO with periodicities of 30–80 years, the comparison of the 40-year running averages of the AMO index and $\delta^{18}O_{SW}$ detailed a significant relationship of 0.5 ($p < 0.001$) (Kilbourne et al., 2008; Wang et al., 2008). Other studies from the Caribbean found the AMO signature in their reconstructed $\delta^{18}O_{SW}$ with strong 60-year cycle (Kilbourne et al., 2008). Time-series analysis with the SSA (Vautard & Ghil, 1989) of our reconstructed $\delta^{18}O_{SW}$ yielded no components in the decadal-interdecadal band that would show a periodicity in the time domain of the AMO even though the correlation between the 40-year moving mean of the AMO index and reconstructed $\delta^{18}O_{SW}$ ratios indicate a robust connection (Figure 6, Figures S2–S5 in Supporting Information S1). Previous studies conducted in the Dry Tortugas have remarked similar results, showing no periodic variation within the record (DeLong et al., 2014). Studies from the Caribbean basin show the AMO cyclicity in $\delta^{18}O_{SW}$ data (Kilbourne et al., 2008). However, recent studies show that those multidecadal oscillations in proxy and instrumental data might actually be artifacts of volcanic activity or other natural and anthropogenic forcings acting together (Mann et al., 2020, 2021). The AMO remains a multidecadal climate mode that is not well understood and might not even be definable by its periodicity. Although no proxy time series in this study shows a significance ($p < 0.05$) in the decadal and interdecadal domain, 25.9% of the variability in the data can be explained by 3–7 years periodicities, as well as 16 years (20.2% of variability in the data is explained by this component) can be observed in the reconstructed $\delta^{18}O_{SW}$. The masking of this signal due to external forcings as described by Mann et al. (2021, 2020) might lead to false periodicities in the 40–70 years band and even near 16 years, so the AMO signal in our proxy records might even be impossible to distinguish from other forcings.

In 1997–1998, a very strong EN event manifested in the eastern Pacific with regional precipitation reaching record levels compared to the 1992 EN event (Xie & Arkin, 1996). There is no corresponding salinity anomaly in the SODA SSS data set for the 1998 EN in our study region; however, reconstructed $\delta^{18}O_{SW}$ indicates a salinity minimum for the northeastern Cuban coast most probably reflecting increased precipitation (Carton & Giese, 2008). A strong positive phase of the NAO started in the early 1990s (Giannini et al., 2001; Visbeck et al., 2001). A positive phase of the NAO counteracts the ENSO-linked precipitation in the GOM due to an increased SLP and a subsequent cooling of the ocean's surface waters (Giannini et al., 2001). The onset of a strong positive NAO phase in 1990 with its climax in 1996 (Visbeck et al., 2001) may have led to a subsequent enhanced winter cooling and therefore less precipitation in the southwestern GOM. Various EN (1968, 1983, 1987, 1992, 1997/1998) and La Niña years (1971, 1975, 1985, 1995) show contradictory $\delta^{18}O_{sw}$ values with certain La Niña years showing a minima in the $\delta^{18}O_{SW}$ record in contrast to what we would expect.

Changes in AMO, ENSO, and NAO are multiple contributing factors affecting SST, SSS, and $\delta^{18}O_{SW}$ values in the GOM. This makes identification of ENSO years in coral $\delta^{18}O_{SW}$ records a challenge for further research.

4. Conclusion

New coral records from the northern coast of Cuba revealed a warming trend in the southeastern GOM from 1845 to 2005. However, the onset of the stagnating trend after the 1980s suggests a reduction in LC strength. This observation was also noted by similar coral studies conducted in the Dry Tortugas in the northern GOM, in addition to model simulations and recent satellite observations (Chollett et al., 2012; DeLong et al., 2014; Liu et al., 2012). The extended gridded SST products of OI-SST and ER-SST suggest a further warming after this pause in warming trend between 1980 and 2005 (Banzon et al., 2014; Huang et al., 2021, 2017). Through our coupled coral Sr/Ca and $\delta^{18}O$ records, the first high-resolution hydroclimate record from the southeastern GOM revealed the onset of a warm AMO phase in the early 1990s. Additionally, two strong EN events in 1992 and 1998 led to an increase in precipitation in the GOM and to freshening conditions. This freshening was observed as strongly depleted coral-based reconstructed $\delta^{18}O_{SW}$ ratios and is in coherence to the gridded SODA SSS (Carton & Giese, 2008). Furthermore, a decrease in salinity coincided with depleted reconstructed $\delta^{18}O_{SW}$ demonstrating the *S. siderea* coral's fidelity as an excellent recorder for hydroclimatology. Due to the scarcity of long-term in situ salinity, precipitation, and temperature records, the reconstructions completed provide additional understanding to the possible teleconnection dynamics in this region due to changes in atmospheric modes of the NAO and AMO.

Data Availability Statement

All data reported in this study trace and minor element ratios and stable isotope ratios have been deposited at the information system PANGAEA (Data Publisher for Earth and Environmental Science) (Harbott et al., 2023). The ER-SST data set is publicly available and was obtained from the IRI/LDEO Climate Data Library (Huang et al., 2017, accessed 1 April 2022). OISSTv2.1 is also publicly available (Banzon et al., 2014; Huang et al., 2021) and was retrieved from U.S. National Oceanic and Atmospheric Association (NOAA) National Centers for Environmental Information (NCEI, https://www.ncei.noaa.gov/products/optimum-interpolation-sst, accessed 1 April 2022). The SODA SSS v2.1.6 (Carton & Giese, 2008) data set was accessed through the IRI/LDEO Climate Library, and is publicly available (http://iridl.ldeo.columbia.edu/SOURCES/.CARTON-GIESE/.SODA/.v2p1p6/, accessed 1 April 2022). The publicly available AMO index times series is based on the Kaplan SST data set (Enfield et al., 2001) and was retrieved from NOAA Physical Science Laboratory (https://psl.noaa.gov/data/timeseries/AMO/, accessed 4 April 2022).

Acknowledgments
We thank the following people for their assistance and support: Sebastian Flotow for coral core sample preparation and microstructure analysis; Jule Mawick, Julia Michaelis, Sahra Greve, and Annalise Povolo for ICP-MS and trace elements analysis; Wolfgang Bevern, Birgit Meyer and Maike Steinkamp for isotope ratio mass spectrometry support; Dr. med. Ralf Windmann and his team at the Zentrum für Moderne Diagnostik (ZEMODI, Bremen, Germany) for their time and patience with coral x-radiograph imaging. Funding for fieldwork and coral core collection was sponsored by the Deutsche Forschungsgemeinschaft (DFG) through grants to TR (RI 1194/2-1, RI 1194/2-2) with local logistical coordination and support from the University of Havana. The OASIS project is funded by the Federal Ministry of Education and Research (BMBF) under the "Make Our Planet Great Again—German Research Initiative," Grant 57429626 to Dr. Henry C. Wu (Junior Research Group Leader), implemented by the German Academic Exchange Service (DAAD). Open Access funding enabled and organized by Projekt DEAL.

References

Alexander, M. A., Halimeda Kilbourne, K., & Nye, J. A. (2014). Climate variability during warm and cold phases of the Atlantic Multidecadal Oscillation (AMO) 1871–2008. *Journal of Marine Systems*, *133*, 14–26. https://doi.org/10.1016/j.jmarsys.2013.07.017

Analytik Jena. (2017). *Inductively Coupled Plasma Plasma Quant Mass Spectrometer: Tech Note PlasmaQuant MS Series: iCRC*. Analyik Jena.

Banzon, V. F., Reynolds, R. W., Stokes, D., & Xue, Y. (2014). A 1/4°-spatial-resolution daily sea surface temperature climatology based on a blended satellite and in situ analysis. *Journal of Climate*, *27*(21), 8221–8228. https://doi.org/10.1175/JCLI-D-14-00293.1

Boers, N. (2021). Observation-based early-warning signals for a collapse of the Atlantic Meridional Overturning Circulation. *Nature Climate Change*, *11*(8), 680–688. https://doi.org/10.1038/s41558-021-01097-4

Caesar, L., McCarthy, G. D., Thornalley, D. J. R., Cahill, N., & Rahmstorf, S. (2021). Current Atlantic Meridional Overturning Circulation weakest in last millennium. *Nature Geoscience*, *14*(3), 118–120. https://doi.org/10.1038/s41561-021-00699-z

Caesar, L., Rahmstorf, S., Robinson, A., Feulner, G., & Saba, V. (2018). Observed fingerprint of a weakening Atlantic Ocean overturning circulation. *Nature*, *556*(7700), 191–196. https://doi.org/10.1038/s41586-018-0006-5

Cai, W., Wu, L., Lengaigne, M., Li, T., McGregor, S., Kug, J.-S., et al. (2019). Pantropical climate interactions. *Science*, *363*(6430), eaav4236. https://doi.org/10.1126/science.aav4236

Carton, J. A., & Giese, B. S. (2008). A reanalysis of ocean climate using Simple Ocean Data Assimilation (SODA). *Monthly Weather Review*, *136*(8), 2999–3017. https://doi.org/10.1175/2007MWR1978.1

Chen, C., & Liu, L.-M. (1993). Joint estimation of model parameters and outlier effects in time series. *Journal of the American Statistical Association*, *88*(421), 284. https://doi.org/10.2307/2290724

Cheng, L., Trenberth, K. E., Fasullo, J., Boyer, T., Abraham, J., & Zhu, J. (2017). Improved estimates of ocean heat content from 1960 to 2015. *Science Advances*, *3*(3), e1601545. https://doi.org/10.1126/sciadv.1601545

Chollett, I., Müller-Karger, F. E., Heron, S. F., Skirving, W., & Mumby, P. J. (2012). Seasonal and spatial heterogeneity of recent sea surface temperature trends in the Caribbean Sea and southeast Gulf of Mexico. *Marine Pollution Bulletin*, *64*(5), 956–965. https://doi.org/10.1016/j.marpolbul.2012.02.016

Dee, S. G., Parsons, L. A., Loope, G. R., Overpeck, J. T., Ault, T. R., & Emile-Geay, J. (2017). Improved spectral comparisons of paleoclimate models and observations via proxy system modeling: Implications for multi-decadal variability. *Earth and Planetary Science Letters*, *476*, 34–46. https://doi.org/10.1016/j.epsl.2017.07.036

DeLong, K. L., Flannery, J. A., Maupin, C. R., Poore, R. Z., & Quinn, T. M. (2011). A coral Sr/Ca calibration and replication study of two massive corals from the Gulf of Mexico. *Palaeogeography, Palaeoclimatology, Palaeoecology*, *307*(1–4), 117–128. https://doi.org/10.1016/j.palaeo.2011.05.005

DeLong, K. L., Flannery, J. A., Poore, R. Z., Quinn, T. M., Maupin, C. R., Lin, K., & Shen, C.-C. (2014). A reconstruction of sea surface temperature variability in the southeastern Gulf of Mexico from 1734 to 2008 C.E. using cross-dated Sr/Ca records from the coral *Siderastrea siderea*. *Paleoceanography*, *29*(5), 403–422. https://doi.org/10.1002/2013PA002524

DeLong, K. L., Quinn, T. M., Taylor, F. W., Shen, C.-C., & Lin, K. (2013). Improving coral-base paleoclimate reconstructions by replicating 350 years of coral Sr/Ca variations. *Palaeogeography, Palaeoclimatology, Palaeoecology*, *373*, 6–24. https://doi.org/10.1016/j.palaeo.2012.08.019

de Villiers, S., Nelson, B. K., & Chivas, A. R. (1995). Biological controls on coral Sr/Ca and δ^{18}O reconstructions of sea surface temperatures. *Science*, *269*(5228), 1247–1249. https://doi.org/10.1126/science.269.5228.1247

Dima, M., Nichita, D. R., Lohmann, G., Ionita, M., & Voiculescu, M. (2021). Early-onset of Atlantic Meridional Overturning Circulation weakening in response to atmospheric CO_2 concentration. *Npj Climate and Atmospheric Science*, *4*(1), 27. https://doi.org/10.1038/s41612-021-00182-x

Enfield, D. B., & Mayer, D. A. (1997). Tropical Atlantic sea surface temperature variability and its relation to El Niño-Southern Oscillation. *Journal of Geophysical Research: Oceans*, *102*(C1), 929–945. https://doi.org/10.1029/96JC03296

Enfield, D. B., Mestas-Nuñez, A. M., & Trimble, P. J. (2001). The Atlantic Multidecadal Oscillation and its relation to rainfall and river flows in the continental U.S. *Geophysical Research Letters*, *28*(10), 2077–2080. https://doi.org/10.1029/2000GL012745

Evans, M. N., Kaplan, A., & Cane, M. A. (2000). Intercomparison of coral oxygen isotope data and historical sea surface temperature (SST): Potential for coral-based SST field reconstructions. *Paleoceanography*, *15*(5), 551–563. https://doi.org/10.1029/2000PA000498

Flower, B. P., & Kennett, J. P. (1990). The Younger Dryas cool episode in the Gulf of Mexico. *Paleoceanography*, *5*(6), 949–961. https://doi.org/10.1029/PA005i006p00949

Fowell, S. E., Sandford, K., Stewart, J. A., Castillo, K. D., Ries, J. B., & Foster, G. L. (2016). Intrareef variations in Li/Mg and Sr/Ca sea surface temperature proxies in the Caribbean reef-building coral *Siderastrea siderea*. *Paleoceanography*, *31*(10), 1315–1329. https://doi.org/10.1002/2016PA002968

Gagan, M. K., Ayliffe, L. K., Beck, J. W., Cole, J. E., Druffel, E. R. M., Dunbar, R. B., & Schrag, D. P. (2000). New views of tropical paleoclimates from corals. *Quaternary Science Reviews*, *19*(1–5), 45–64. https://doi.org/10.1016/S0277-3791(99)00054-2

Gagan, M. K., Ayliffe, L. K., Hopley, D., Cali, J. A., Mortimer, G. E., Chappell, J., et al. (1998). Temperature and surface-ocean water balance of the mid-Holocene Tropical Western Pacific. *Science*, *279*(5353), 1014–1018. https://doi.org/10.1126/science.279.5353.1014

Giannini, A., Cane, M. A., & Kushnir, Y. (2001). Interdecadal changes in the ENSO teleconnection to the Caribbean region and the North Atlantic Oscillation. *Journal of Climate*, *14*(13), 2867–2879. https://doi.org/10.1175/1520-0442(2001)014<2867:ICITET>2.0.CO;2

Giannini, A., Kushnir, Y., & Cane, M. A. (2000). Interannual variability of Caribbean rainfall, ENSO, and the Atlantic Ocean. *Journal of Climate*, *13*(2), 297–311. https://doi.org/10.1175/1520-0442(2000)013<0297:IVOCRE>2.0.CO;2

Giry, C., Felis, T., Kölling, M., Scholz, D., Wei, W., Lohmann, G., & Scheffers, S. (2012). Mid- to late Holocene changes in tropical Atlantic temperature seasonality and interannual to multidecadal variability documented in southern Caribbean corals. *Earth and Planetary Science Letters*, *331–332*, 187–200. https://doi.org/10.1016/j.epsl.2012.03.019

Goly, A., & Teegavarapu, R. S. V. (2014). Individual and coupled influences of AMO and ENSO on regional precipitation characteristics and extremes. *Water Resources Research*, *50*(6), 4686–4709. https://doi.org/10.1002/2013WR014540

Gordon, A. L. (1967). Circulation of the Caribbean Sea. *Journal of Geophysical Research*, *72*(24), 6207–6223. https://doi.org/10.1029/jz072i024p06207

Guzmán, H., & Tudhope, A. (1998). Seasonal variation in skeletal extension rate and stable isotopic (^{13}C/^{12}C and ^{18}O/^{16}O) composition in response to several environmental variables in the Caribbean reef coral *Siderastrea siderea*. *Marine Ecology Progress Series*, *166*, 109–118. https://doi.org/10.3354/meps166109

Harbott, M., Wu, H. C., Kuhnert, H., Jimenez, C., González-Díaz, P., & Rixen, T. (2023). Stable isotope and trace element data for a *Siderastrea siderea* coral core CIM_C_2-2-1/CIM_C_2-2-2 from the Gulf of Mexico [Dataset]. PANGAEA. https://doi.org/10.1594/PANGAEA.963278

Howell, P., Pisias, N., Ballance, J., Baughman, J., & Ochs, L. (2006). *ARAND time-series analysis software* (p. 685). Brown University.

Huang, B., Liu, C., Banzon, V., Freeman, E., Graham, G., Hankins, B., et al. (2021). Improvements of the Daily Optimum Interpolation Sea Surface Temperature (DOISST) Version 2.1. *Journal of Climate*, *34*(8), 2923–2939. https://doi.org/10.1175/JCLI-D-20-0166.1

Huang, B., Thorne, P. W., Banzon, V. F., Boyer, T., Chepurin, G., Lawrimore, J. H., et al. (2017). Extended Reconstructed Sea Surface Temperature, Version 5 (ERSSTv5): Upgrades, validations, and intercomparisons. *Journal of Climate*, *30*(20), 8179–8205. https://doi.org/10.1175/JCLI-D-16-0836.1

Hughes, T. P., Anderson, K. D., Connolly, S. R., Heron, S. F., Kerry, J. T., Lough, J. M., et al. (2018). Spatial and temporal patterns of mass bleaching of corals in the Anthropocene. *Science*, *359*(6371), 80–83. https://doi.org/10.1126/science.aan8048

Hyndman, R. J., & Athanasopoulos, G. (2018). *Forecasting: Principles and practice*. OTexts.

Intergovernmental Panel On Climate Change. (2023). *Climate change 2021—The physical science basis: Working Group I Contribution to the Sixth Assessment Report of the Intergovernmental Panel on Climate Change* (1st ed.). Cambridge University Press. https://doi.org/10.1017/9781009157896

Jury, M., Malmgren, B. A., & Winter, A. (2007). Subregional precipitation climate of the Caribbean and relationships with ENSO and NAO. *Journal of Geophysical Research*, *112*(D16), D16107. https://doi.org/10.1029/2006JD007541

Kilbourne, K. H., Quinn, T. M., Webb, R., Guilderson, T., Nyberg, J., & Winter, A. (2008). Paleoclimate proxy perspective on Caribbean climate since the year 1751: Evidence of cooler temperatures and multidecadal variability: Caribbean climate of the last 250 years. *Paleoceanography*, *23*(3), n/a. https://doi.org/10.1029/2008PA001598

LeGrande, A. N., & Schmidt, G. A. (2006). Global gridded data set of the oxygen isotopic composition in seawater. *Geophysical Research Letters*, *33*(12), L12604. https://doi.org/10.1029/2006GL026011

Liu, Y., Lee, S.-K., Muhling, B. A., Lamkin, J. T., & Enfield, D. B. (2012). Significant reduction of the Loop Current in the 21st century and its impact on the Gulf of Mexico: Future warming of the GOM. *Journal of Geophysical Research: Oceans*, *117*(C5), n/a. https://doi.org/10.1029/2011JC007555

Lough, J. M. (2004). A strategy to improve the contribution of coral data to high-resolution paleoclimatology. *Palaeogeography, Palaeoclimatology, Palaeoecology*, *204*(1–2), 115–143. https://doi.org/10.1016/S0031-0182(03)00727-2

Lowenstam, H. A., & Epstein, S. (1957). On the origin of sedimentary aragonite needles of the Great Bahama Bank. *The Journal of Geology*, *65*(4), 364–375. https://doi.org/10.1086/626439

Lund, D. C., & Curry, W. B. (2004). Late Holocene variability in Florida Current surface density: Patterns and possible causes: Late Holocene Florida Current δ^{18}O. *Paleoceanography*, *19*(4), n/a. https://doi.org/10.1029/2004PA001008

Mann, M. E., Steinman, B. A., Brouillette, D. J., & Miller, S. K. (2021). Multidecadal climate oscillations during the past millennium driven by volcanic forcing. *Science*, *371*(6533), 1014–1019. https://doi.org/10.1126/science.abc5810

Mann, M. E., Steinman, B. A., & Miller, S. K. (2020). Absence of internal multidecadal and interdecadal oscillations in climate model simulations. *Nature Communications*, *11*(1), 49. https://doi.org/10.1038/s41467-019-13823-w

Maupin, C. R., Quinn, T. M., & Halley, R. B. (2008). Extracting a climate signal from the skeletal geochemistry of the Caribbean coral *Siderastrea siderea*. *Geochemistry, Geophysics, Geosystems*, *9*(12), n/a. https://doi.org/10.1029/2008GC002106

Otto, S. A. (2019). Comparison of change point detection methods [Blog post]. Retrieved from https://www.marinedatascience.co/blog/2019/09/28/comparison-of-changepoint-detection-methods/

Piecuch, C. G. (2020). Likely weakening of the Florida Current during the past century revealed by sea-level observations. *Nature Communications*, *11*(1), 3973. https://doi.org/10.1038/s41467-020-17761-w

Poore, R. Z., DeLong, K. L., Richey, J. N., & Quinn, T. M. (2009). Evidence of multidecadal climate variability and the Atlantic Multidecadal Oscillation from a Gulf of Mexico sea-surface temperature-proxy record. *Geo-Marine Letters*, *29*(6), 477–484. https://doi.org/10.1007/s00367-009-0154-6

Ren, L., Linsley, B. K., Wellington, G. M., Schrag, D. P., & Hoegh-guldberg, O. (2003). Deconvolving the δ^{18}O seawater component from subseasonal coral δ^{18}O and Sr/Ca at Rarotonga in the southwestern subtropical Pacific for the period 1726 to 1997. *Geochimica et Cosmochimica Acta*, *67*(9), 1609–1621. https://doi.org/10.1016/S0016-7037(02)00917-1

Reynolds, R. W., Rayner, N. A., Smith, T. M., Stokes, D. C., & Wang, W. (2002). An improved in situ and satellite SST analysis for climate. *Journal of Climate*, *15*(13), 1609–1625. https://doi.org/10.1175/1520-0442(2002)015<1609:AIISAS>2.0.CO;2

Richey, J. N., Poore, R. Z., Flower, B. P., & Quinn, T. M. (2007). 1400 yr multiproxy record of climate variability from the northern Gulf of Mexico. *Geology*, *35*(5), 423. https://doi.org/10.1130/G23507A.1

Richey, J. N., Poore, R. Z., Flower, B. P., Quinn, T. M., & Hollander, D. J. (2009). Regionally coherent Little Ice Age cooling in the Atlantic Warm Pool. *Geophysical Research Letters*, *36*(21), L21703. https://doi.org/10.1029/2009GL040445

Rodriguez, L. G., Cohen, A. L., Ramirez, W., Oppo, D. W., Pourmand, A., Edwards, R. L., et al. (2019). Mid-Holocene, coral-based sea surface temperatures in the Western Tropical Atlantic. *Paleoceanography and Paleoclimatology*, *34*(7), 1234–1245. https://doi.org/10.1029/2019PA003571

Roemmich, D., John Gould, W., & Gilson, J. (2012). 135 years of global ocean warming between the Challenger expedition and the Argo Programme. *Nature Climate Change*, *2*(6), 425–428. https://doi.org/10.1038/nclimate1461

Schmidt, M. W., Weinlein, W. A., Marcantonio, F., & Lynch-Stieglitz, J. (2012). Solar forcing of Florida Straits surface salinity during the early Holocene. *Paleoceanography*, *27*(3), n/a. https://doi.org/10.1029/2012PA002284

Schrag, D. P. (1999). Rapid analysis of high-precision Sr/Ca ratios in corals and other marine carbonates. *Paleoceanography*, *14*(2), 97–102. https://doi.org/10.1029/1998PA900025

Smeed, D. A., Josey, S. A., Beaulieu, C., Johns, W. E., Moat, B. I., Frajka-Williams, E., et al. (2018). The North Atlantic Ocean is in a state of reduced overturning. *Geophysical Research Letters*, *45*(3), 1527–1533. https://doi.org/10.1002/2017GL076350

Smith, S. V., Buddemeier, R. W., Redalje, R. C., & Houck, J. E. (1979). Strontium-calcium thermometry in coral skeletons. *Science*, *204*(4391), 404–407. https://doi.org/10.1126/science.204.4391.404

Thompson, D. M., Ault, T. R., Evans, M. N., Cole, J. E., & Emile-Geay, J. (2011). Comparison of observed and simulated tropical climate trends using a forward model of coral δ^{18}O: Comparison of tropical climate trends. *Geophysical Research Letters*, *38*(14), n/a. https://doi.org/10.1029/2011GL048224

Vásquez-Bedoya, L. F., Cohen, A. L., Oppo, D. W., & Blanchon, P. (2012). Corals record persistent multidecadal SST variability in the Atlantic Warm Pool since 1775 AD: Tropical Atlantic SST since 1775 AD. *Paleoceanography*, *27*(3), n/a. https://doi.org/10.1029/2012PA002313

Vautard, R., & Ghil, M. (1989). Singular spectrum analysis in nonlinear dynamics, with applications to paleoclimatic time series. *Physica D: Nonlinear Phenomena*, *35*(3), 395–424. https://doi.org/10.1016/0167-2789(89)90077-8

Visbeck, M. H., Hurrell, J. W., Polvani, L., & Cullen, H. M. (2001). The North Atlantic Oscillation: Past, present, and future. *Proceedings of the National Academy of Sciences*, *98*(23), 12876–12877. https://doi.org/10.1073/pnas.231391598

Wang, C., Lee, S.-K., & Enfield, D. B. (2008). Atlantic Warm Pool acting as a link between Atlantic Multidecadal Oscillation and Atlantic tropical cyclone activity: Atlantic tropical cyclone activity. *Geochemistry, Geophysics, Geosystems*, *9*(5), n/a. https://doi.org/10.1029/2007GC001809

Weerabaddana, M. M., DeLong, K. L., Wagner, A. J., Loke, D. W. Y., Kilbourne, K. H., Slowey, N., et al. (2021). Insights from barium variability in a *Siderastrea siderea* coral in the northwestern Gulf of Mexico. *Marine Pollution Bulletin*, *173*, 112930. https://doi.org/10.1016/j.marpolbul.2021.112930

Wolter, K., & Timlin, M. S. (2011). El Niño/Southern Oscillation behaviour since 1871 as diagnosed in an extended multivariate ENSO index (MEI.ext). *International Journal of Climatology*, *31*(7), 1074–1087. https://doi.org/10.1002/joc.2336

Xie, P., & Arkin, P. A. (1996). Analyses of global monthly precipitation using gauge observations, satellite estimates, and numerical model predictions. *Journal of Climate*, *9*(4), 840–858. https://doi.org/10.1175/1520-0442(1996)009<0840:aogmpu>2.0.co;2

Xu, Y.-Y., Pearson, S., & Halimeda Kilbourne, K. (2015). Assessing coral Sr/Ca–SST calibration techniques using the species Diploria strigosa. *Palaeogeography, Palaeoclimatology, Palaeoecology*, *440*, 353–362. https://doi.org/10.1016/j.palaeo.2015.09.016

Yu, J.-Y., Kao, P., Paek, H., Hsu, H.-H., Hung, C., Lu, M.-M., & An, S.-I. (2015). Linking emergence of the Central Pacific El Niño to the Atlantic Multidecadal Oscillation. *Journal of Climate*, *28*(2), 651–662. https://doi.org/10.1175/JCLI-D-14-00347.1

Zeileis, A., Leisch, F., Hornik, K., & Kleiber, C. (2002). strucchange: An R package for testing for structural change in linear regression models. *Journal of Statistical Software*, *7*(2). https://doi.org/10.18637/jss.v007.i02

References From the Supporting Information

DeCarlo, T. M., Gaetani, G. A., Cohen, A. L., Foster, G. L., Alpert, A. E., & Stewart, J. A. (2016). Coral Sr-U thermometry. *Paleoceanography*, *31*(6), 626–638. https://doi.org/10.1002/2015PA002908

DeCarlo, T. M., Gaetani, G. A., Holcomb, M., & Cohen, A. L. (2015). Experimental determination of factors controlling U/Ca of aragonite precipitated from seawater: Implications for interpreting coral skeleton. *Geochimica et Cosmochimica Acta*, *162*, 151–165. https://doi.org/10.1016/j.gca.2015.04.016

Montagna, P., McCulloch, M., Douville, E., López Correa, M., Trotter, J., Rodolfo-Metalpa, R., et al. (2014). Li/Mg systematics in scleractinian corals: Calibration of the thermometer. *Geochimica et Cosmochimica Acta*, *132*, 288–310. https://doi.org/10.1016/j.gca.2014.02.005

Nurhati, I. S., Cobb, K. M., & Di Lorenzo, E. (2011). Decadal-scale SST and salinity variations in the central tropical Pacific: Signatures of natural and anthropogenic climate change. *Journal of Climate*, *24*(13), 3294–3308. https://doi.org/10.1175/2011JCLI3852.1